Journal of Power Sources 196 (2011) 6809–6814

Contents lists available at ScienceDirect

Journal of Power Sources

journal homepage: www.elsevier.com/locate/jpowsour

Structure and electrode reactions of layered rocksalt $LiFeO_2$ nanoparticles for lithium battery cathode

Masaaki Hirayama*, Hiroki Tomita, Kei Kubota, Ryoji Kanno

Department of Electronic Chemistry, Interdisciplinary Graduate School of Science and Engineering, Tokyo Institute of Technology, 4259 Nagatsuta, Midori-ku, Yokohama, 226-8502, Japan

ARTICLE INFO

Article history:
Received 12 August 2010
Received in revised form
30 September 2010
Accepted 2 October 2010
Available online 8 October 2010

Keywords:
Lithium iron oxide
Nanosize effect
Ion exchange
α-$NaFeO_2$
Lithium batteries

ABSTRACT

Lithium iron oxide nanoparticles with the layered rocksalt structure (*O*3-$LiFeO_2$) were synthesized by ion exchange from size-controlled α-$NaFeO_2$ particles. 40-nm-sized *O*3-$LiFeO_2$ exhibited intercalation characteristics for cell voltages in the range 2.0–4.5 V. A plateau region around 4 V was observed in the first charge curve. Mechanistic studies using Mössbauer spectroscopy and X-ray diffraction measurements revealed that the oxidation state of Fe did not change and that a phase transition from rhombohedral to cubic symmetry occurred during the initial charging process, indicating oxygen release with lithium deintercalation. The cubic phase showed a reversible charge/discharge capacity. To investigate the detailed mechanism, $LiFeO_{2-d}$ with oxygen-vacancy defects was directly synthesized using CaH_2 as a reducing agent. The phase with oxygen-vacancy defects contained a larger amount of the cubic phase and had a narrower plateau region during the first charge cycle than $LiFeO_2$ nanoparticles, which is similar to $LiFeO_2$ nanoparticles after initial charging. These results demonstrate that the extraction of oxygen leads to the cation-distribution changes in $LiFeO_2$ during the initial charge process.

1. Introduction

Lithium transition-metal oxides Li*M*O_2 (*M* = Mn, Co, Ni, etc.) with the layered rocksalt structure are commercially produced as a cathode material for rechargeable lithium batteries. The layered rocksalt (*O*3-type) structure has an oxygen stacking sequence of *ABCABC* along the *c*-axis and undergoes rapid lithium intercalation [1]. Generally, the structure of Li*M*O_2 depends primarily on the size of the *M* cation [2]. Compounds containing smaller *M* cations (*M* = V, Cr, Co, Ni) adopt the layered rocksalt structure, whereas compounds with larger *M* cations (*M* = Fe, Ti) tend to adopt the disordered rocksalt structure or the tetragonally ordered structure. The boundary between these structures is located between V^{3+} and Fe^{3+} when conventional high-temperature ceramic sintering techniques are used. However, layered *O*3-type $LiFeO_2$ (*O*3-$LiFeO_2$) has been synthesized by an ion-exchange reaction with α-$NaFeO_2$ [2,3] and a hydrothermal reaction [4]. *O*3-$LiFeO_2$ is a promising cathode material as it has a low toxicity and is cheaper than Li*M*O_2 (*M* = Mn, Co, Ni). However, its electrochemical characteristics have not been obtained [4].

Nanomaterials have been attracting considerable interest for use in electrodes because they have unique reaction mechanisms. For example, iron oxides (Fe_2O_3) nanoparticles exhibit electrochemical activity, whereas micro-sized Fe_2O_3 do not show intercalation/deintercalation properties [5,6]. *O*3-$LiFeO_2$ nanoparticles are expected to readily undergo electrochemical lithium intercalation. Recently, we have succeeded to synthesize *O*3-$LiFeO_2$ nanoparticles by an ion exchange reaction using α-$NaFeO_2$ nanoparticles [7,8]. The *O*3-$LiFeO_2$ nanoparticles underwent reversible lithium intercalation with a discharge capacity over 100 mAh g^{-1}. Structural investigation is needed to clarify electrode reactions of the *O*3-$LiFeO_2$ nanoparticles. In this study, the *O*3-$LiFeO_2$ nanoparticles were characterized by X-ray diffraction (XRD), scanning electron microscopy (SEM), Mössbauer spectroscopy, and electrochemical measurements. A plateau region observed during the first charge curve, XRD patterns, and Mössbauer spectra indicate an irreversible phase transition to a rocksalt-type phase due to oxygen-vacancy deficiencies during the electrochemical process. To investigate the detailed reaction mechanism of $LiFeO_2$ electrodes, a phase with oxygen vacancies $LiFeO_{2-d}$ was synthesized directly using CaH_2 as the reducing agent and its structural and electrochemical characteristics were compared with those of $LiFeO_2$ after electrochemical reactions.

2. Experimental

*O*3-$LiFeO_2$ nanoparticles were synthesized by an ion exchange reaction from α-$NaFeO_2$ nanoparticles prepared by solid-state

* Corresponding author. Tel.: +81 459245570; fax: +81 459245409.
E-mail address: hirayama@echem.titech.ac.jp (M. Hirayama).

0378-7753/$ – see front matter © 2010 Elsevier B.V. All rights reserved.
doi:10.1016/j.jpowsour.2010.10.009

Table 1
IS and QS for pristine 40 nm *O*3-$LiFeO_2$ obtained by Mössbauer spectrum analysis.

	I.S./mm s^{-1}	Q.S./mm s^{-1}	Ratio (%)
Fe^{3+} (1)	0.356	0.456	64
Fe^{3+} (2)	0.334	0.821	36
*O*3-type $LiFeO_2$ [Ref. [2]]	0.360	0.405	
Ordered rocksalt type $LiFeO_2$ [Ref. [2]]	0.359	1.089	

and hydrothermal reactions. The synthesis conditions for α-$NaFeO_2$ precursors and *O*3-$LiFeO_2$ nanoparticles were described our previous report [7,8]. An oxygen-deficient phase $LiFeO_{2-d}$ was synthesized using a CaH_2 as a reducing agent [9,10]. $LiFeO_2$ nanoparticles were mixed with twice the amount of CaH_2 powder in a glass tube in an argon-filled glove box and the tube was vacuum sealed and then heated at 190 °C for 24 h. The products and any unreacted CaH_2 were removed by rinsing in dehydrated ethanol containing 1-M NH_4Cl.

XRD patterns of powdered samples were obtained using two X-ray diffractometers (Rigaku, RU-200B and Ultima IV). The structural and profile parameters were refined by Rietveld analysis using the RIETAN-2000 computer software [11] and RIETAN-FP [12]. The structural parameters were refined using a two-phase model with space groups of *R*-3*m* and *Fd*-3*m*. The pseudo-Voigt function was used to fit the peak profiles. The particle texture was observed by SEM (Jeol, JSM-6510).

Electrochemical intercalation and deintercalation reactions were performed using a 2032-type cell with a lithium metal anode. The working electrode was a mixture of the obtained sample/ECP/PVdF with a weight ratio of 60/40/6. The electrolyte was a 1-M solution of $LiPF_6$ in a 30:70 mixture of ethylene carbonate and diethyl carbonate by volume.

Mössbauer spectra were obtained using with a Mössbauer spectrometer (Topologic System Inc.) using a ^{57}Co γ-ray source. The spectrometer was calibrated using α-Fe as a standard. The data were analyzed using Mosswin (ver. 3.0) software.

3. Results and discussion

3.1. Structural characterization of *O*3-$LiFeO_2$ nanoparticles

Fig. 1 shows the XRD pattern and SEM image of $LiFeO_2$ synthesized by ion-exchange reaction with α-$NaFeO_2$ nanoparticles that had been prepared by a hydrothermal reaction and had particle sizes of 19 nm [7,8]. The diffraction peaks can be assigned to the layered rocksalt structure with a space group of *R*-3*m*. The $LiFeO_2$ particles had the particle size distribution of 20–300 nm and the average particle size of 40 nm. The XRD and SEM results confirm the formation of $LiFeO_2$ nanoparticles. Fig. 2 shows a Mössbauer spectrum of the 40-nm *O*3-$LiFeO_2$ particles. Fitting the spectrum with two hyperfine components provided the best agreement with the experimental results. Table 1 lists the obtained parameter values. The spectrum consists of two quadrupole doublets with a relative abundance of 64:36, indicating two iron-containing phases with different coordination environments around the iron ion. The isomer shifts (IS) for both components are characteristic of the Fe^{3+} ion in *O*3-$LiFeO_2$. Shirane et al. reported the IS and quadrupole splittings (QS) of *O*3-$LiFeO_2$ and ordered rocksalt type $LiFeO_2$ [2]. The QSs of the major and minor components, Fe^{3+}(1) and Fe^{3+}(2), are similar to those of *O*3-$LiFeO_2$ and ordered rocksalt type $LiFeO_2$, respectively. This result reveals that cation mixing between lithium and iron ions occurred in 40-nm *O*3-$LiFeO_2$ during the ion-exchange process and that the ordered rocksalt phase was then formed. The formation of ordered rocksalt type $LiFeO_2$ is consistent with the additional peak at 30° in the XRD patterns, which could be

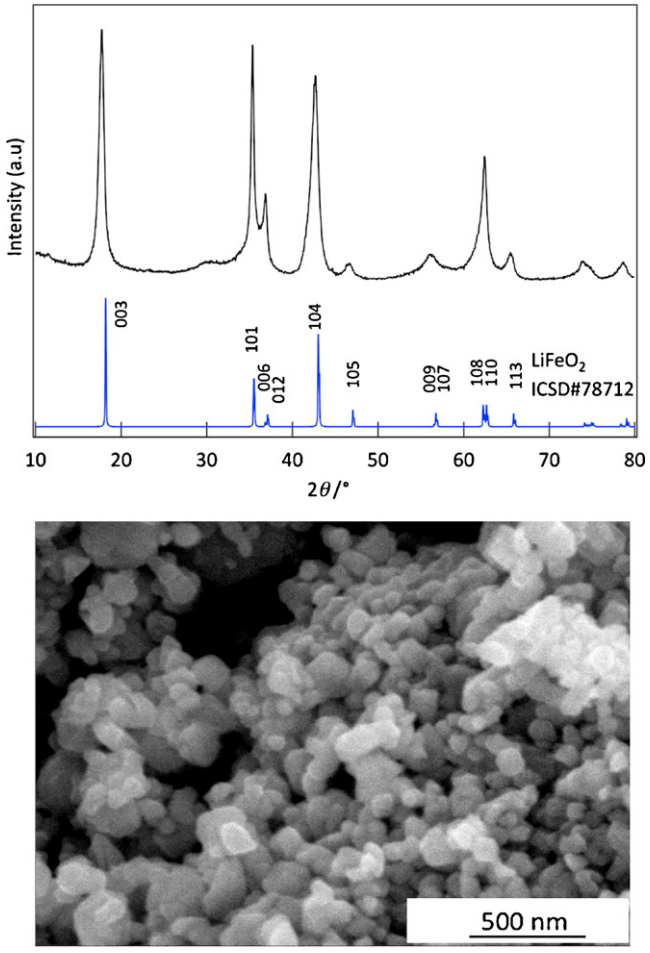

Fig. 1. XRD pattern and SEM image of *O*3-$LiFeO_2$ synthesized by an ion-exchange reaction of $NaFeO_2$ prepared by a hydrothermal reaction. Simulation XRD pattern of $LiFeO_2$ based on ICSD data are also shown.

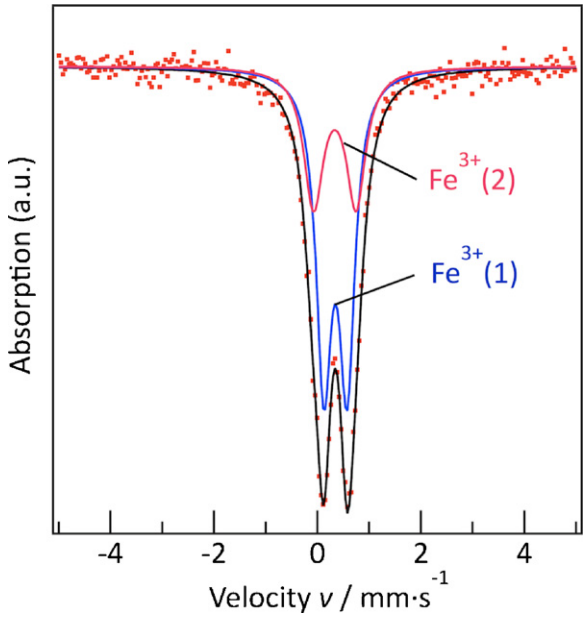

Fig. 2. Mössbauer spectrum of 40-nm-sized $LiFeO_2$. The velocity scale is relative to a pure Fe absorber. A fitting curve for a two-component model is also shown.

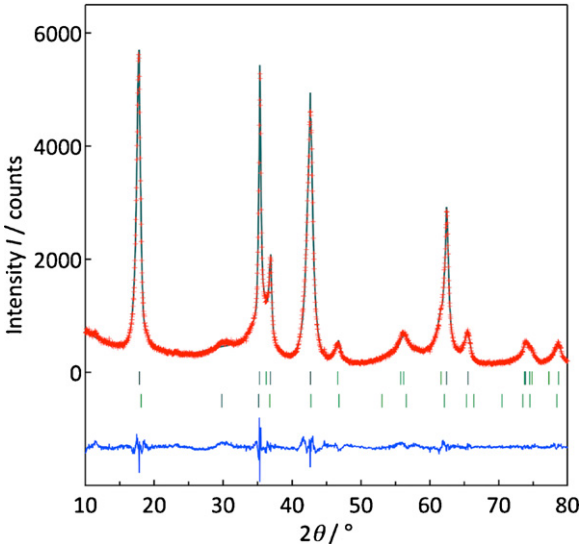

Fig. 3. Rietveld analysis of 40-nm-sized $LiFeO_2$. The observed intensity data are depicted by dots while the solid line overlying them is the calculated intensity. Vertical markers below the diffraction patterns indicate positions of possible Bragg reflections. Differences between the observed and calculated intensities are plotted as D_{yi} at the bottom using the same scale.

the 220 reflection. Therefore, we performed Rietveld analysis of the obtained $LiFeO_2$ using a two-phase model consisting of *O*3-$LiFeO_2$ and ordered rocksalt type $LiFeO_2$. Fig. 3 shows typical Rietveld analysis results for 40-nm *O*3-$LiFeO_2$. The two-phase model was found to provide better fitting for the XRD pattern than the single-phase *O*3-$LiFeO_2$ model. Table 2 summarizes the refined parameters. The lithium ions in *O*3-$LiFeO_2$ are located at the 3*a* and 3*b* sites with proportions of 86% and 14%, respectively. This distribution suggests cation mixing of lithium and iron ions under the high intercalation reaction field during the ion-exchange process. The mass fraction of *O*3-$LiFeO_2$ to the ordered rocksalt type $LiFeO_2$ is 0.637/0.363, which is consistent with the relative abundance obtained from the Mössbauer spectrum. The cation distribution might cause the phase transition to the ordered rocksalt type $LiFeO_2$.

3.2. Electrochemical properties of *O*3-$LiFeO_2$ nanoparticles

Fig. 4a shows charge–discharge curves of *O*3-$LiFeO_2$ nanoparticles. The *O*3-$LiFeO_2$ nanoparticles exhibited a discharge capacity of over 100 mAh g^{-1}. Ado et al. found that *O*3-$LiFeO_2$ microparticles had a slight electrochemical capacity of 8 mAh g^{-1} at a current density of 2 mAh g^{-1} [4]. They suggested that iron ions at the lithium site (3*a*) obstruct the lithium diffusion pathway. The electrochemical activity of the present 40-nm *O*3-$LiFeO_2$ with cation disordering suggests that nanosize effects affect the lithium diffusion such as by reducing the diffusion pathway and increasing the surface area. Whereas a plateau around the 4 V region was observed during the first charge process, it disappeared in the second charge process. Furthermore, a new plateau gradually appeared around the 3 V region during electrochemical cycling. These results suggest an irreversible phase transition of $LiFeO_2$ nanoparticles during the first charge process and following cycles. Fig. 4b shows the variation in the discharge capacity of $LiFeO_2$ nanoparticles. The discharge capacity increased with the cycle number. The new phase exhibited a larger discharge capacity (about 120 mAh g^{-1}) than the pristine $LiFeO_2$ phase (about 90 mAh g^{-1}). The average voltage of the discharge curve increased from 2.83 V for the first discharge to 2.95 V for the 23rd discharge.

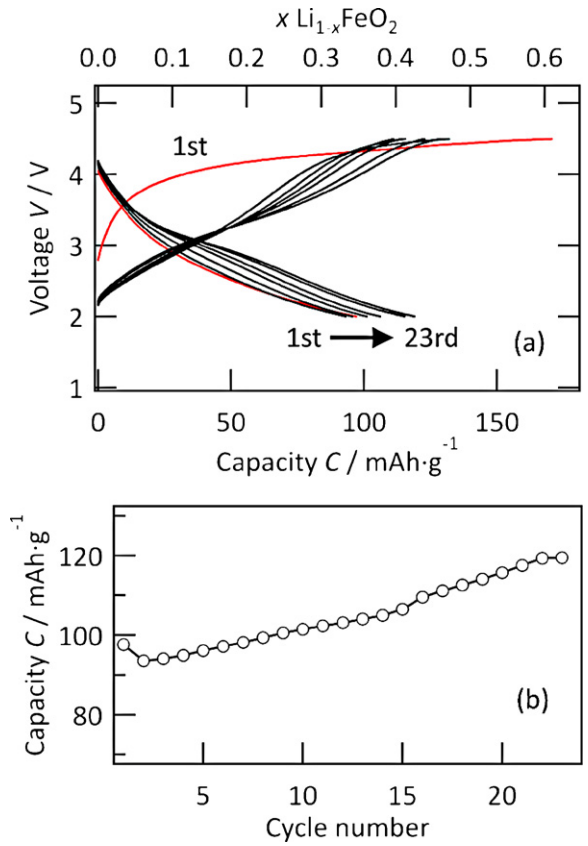

Fig. 4. Charge/discharge curves and discharge capacities of 40-nm-sized $LiFeO_2$ nanoparticles. The current density is 10 mA g^{-1} (1/28 C).

Table 2
Rietveld refinement results for 40-nm-sized $LiFeO_2$.

Atom	Site	*g*	*x*	*y*	*z*	B_{eq}/Å^2
Phase 1 rhombohedral $LiFeO_2$						
Li(1)	3*a*	=*g*(Fe(1))	0	0	0	1.3(11)
Li(2)	3*b*	=1 − *g*(Fe(1))	0	0	0.5	=*B*(Li(1))
Fe(1)	3*b*	0.86(2)	0	0	0.5	0.36(10)
Fe(2)	3*a*	=1 − *g*(Fe(1))	0	0	0	=*B*(Fe(1))
O(1)	6*c*	1	0	0	0.240(2)	1.10(8)
Phase 2 ordered rocksalt $LiFeO_2$						
Li (3)	16*c*	1	0.125	0.125	0.125	=*B*(Li(1))
Fe(3)	16*d*	1	0.625	0.625	0.625	=*B*(Fe(1))
O(2)	32*e*	1	0.372(11)	=*x*(O(2))	=*x*(O(2))	=*B*(O(1))

Space group *R*-3m, $a = 2.9754(8)$ Å, $c = 14.821(5)$ Å, $R_I = 0.64$, $R_F = 0.33$.
Space group *Fd*-3*m*, $a = 8.447\ (12)$ Å, $R_I = 0.85$, $R_F = 0.36$.
$R_{wp} = 5.96\%$, $R_p = 4.46\%$, $R_e = 3.95\%$, $S = R_{wp}/R_e = 1.50$.
Mass fraction (weight%) phase1:phase2 = 0.637:0.363.

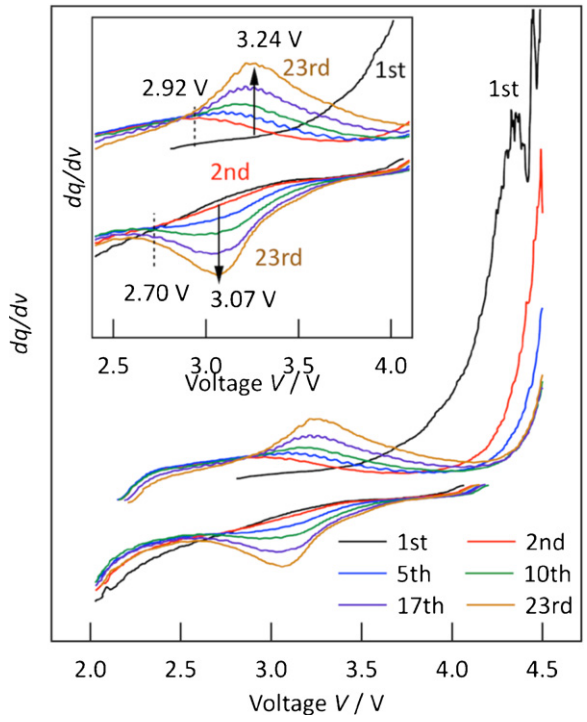

Fig. 5. Differential capacity plots of 40-nm-sized $LiFeO_2$ obtained from the charge/discharge curves shown in Fig. 4a.

Fig. 5 shows dQ/dV plots versus cell voltage for 40-nm $LiFeO_2$. In the first charge process, no anodic peak was observed between 3 V and 4 V in the first charge process, and an anodic peak due to the plateau region was observed at 4.3 V. As an anodic peak attributed to decomposition of the EC/DEC electrolyte appears above 4.3 V, the anodic peak at 4.3 V suggests a phase change of the $LiFeO_2$ nanoparticles. In the second charge process, broad anodic and cathodic peaks were observed at 2.92 and 2.70 V, respectively. In following cycles, new anodic and cathodic peaks appeared at 3.24 and 3.07 V, respectively. The peak intensities of the anodic and cathodic peaks gradually increased with the cycle number. The reaction voltage changed during the electrochemical cycling. This result is consistent with the emergence of the 3 V plateau region in the charge/discharge curves. The charge/discharge and dQ/dV curves suggest that the phase changes in the $LiFeO_2$ nanoparticles occur in two stages; the first charge process and the following process.

3.3. *Electrode reactions of O3-$LiFeO_2$ nanoparticles*

A plateau region during the first charge has been reported for a Li_2MnO_3 cathode typically above 4.5 V and has been attributed to removal of Li_2O from Li_2MnO_3 [13,14]. The $Li_{2-2x}MnO_{3-x}$ phase exhibits a larger discharge capacity (about 200 mAh g^{-1}) than the original Li_2MnO_3 (only 20 mAh g^{-1}). This fact demonstrates an importance of structural changes during the initial battery reaction to obtain a higher electrochemical-activity of electrodes at following cycles. The wide plateau region in the first charge curve for the *O*3-$LiFeO_2$ nanoparticles indicates a phase change from *O*3-$LiFeO_2$ to a lithium and oxygen deficient phase that could exhibit the reversible lithium intercalation behavior. Considering the slight electrochemical capacity of the *O*3-$LiFeO_2$ microparticles, the initial structural change could be stimulated with decreasing particle size of *O*3-$LiFeO_2$.

The phase change of *O*3-$LiFeO_2$ nanoparticles at the first charge was investigated by ex situ XRD and Mössbauer measurements. Fig. 6 shows the structural changes of 40-nm $LiFeO_2$ after being

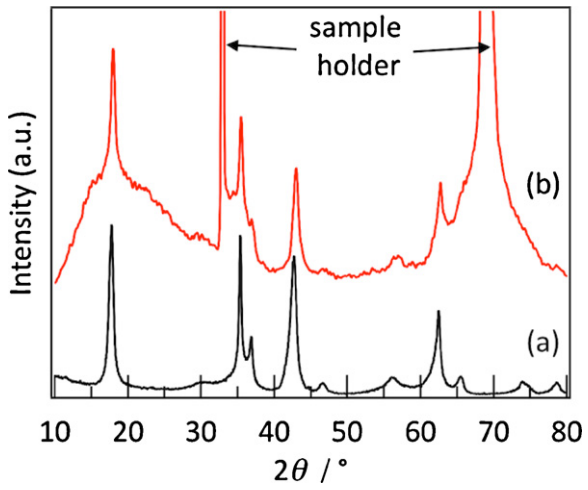

Fig. 6. XRD patterns of 40-nm $LiFeO_2$: (a) pristine and (b) after being charged to 4.5 V at the first cycle.

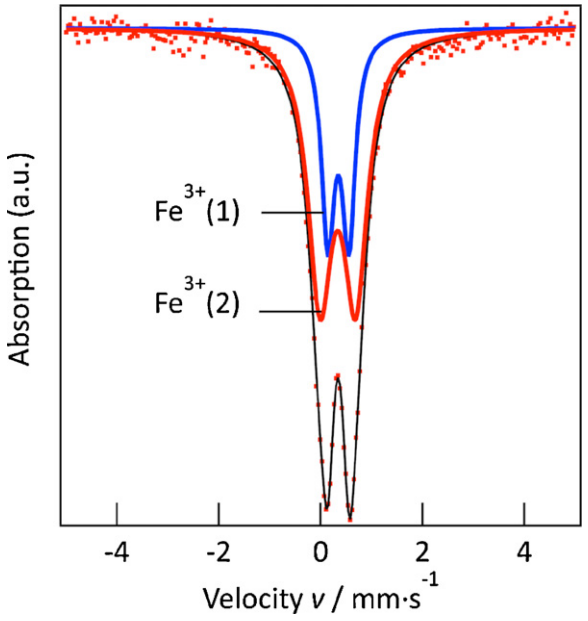

Fig. 7. Mössbauer spectrum of 40-nm $LiFeO_2$ after it had been charged to 4.5 V.

charged to 4.5 V at the first cycle. The $LiFeO_2$ peaks shifted to higher angles. The lattice constants decreased from $a = 2.9754(8)$ and $c = 14.821(5)$ Å for the pristine sample to $a = 2.955(2)$ and $c = 14.63(2)$ Å for the charged sample. Fig. 7 shows a Mössbauer spectrum of 40-nm *O*3-$LiFeO_2$ after it had been charged to 4.5 V. Spectral fitting assuming two hyperfine components gives the best agreement with the experimental result. Table 3 lists the parameter values obtained. The Mössbauer spectrum of pristine $LiFeO_2$ with a particle size of 40-nm indicates two types of Fe^{3+} with different QS with a ratio of 64:36; this ratio changed to 30:70 after charging to 4.5 V. This indicates the phase transition from the layered rocksalt $LiFeO_2$ to an ordered rocksalt $LiFeO_2$. No components

Table 3
IS and QS for $LiFeO_2$ after it had been charged to 4.5 V obtained by Mössbauer spectral analysis.

	I.S./mm s^{-1}	Q.S./mm s^{-1}	Ratio (%)
Fe^{3+} (1)	0.347	0.409	30
Fe^{3+} (2)	0.336	0.700	70

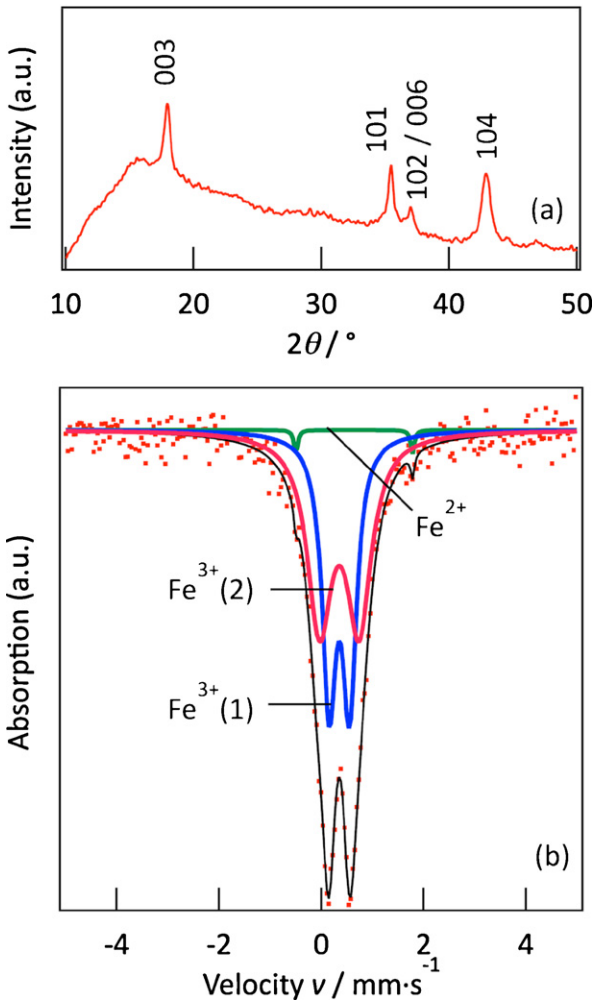

Fig. 8. XRD pattern (a) and Mössbauer spectrum (b) of 40-nm-sized $LiFeO_2$ after reduction by CaH_2 at 190 °C. The velocity scale is relative to a pure Fe absorber. A fitting curve for a three-component model is also shown.

of Fe^{4+} were observed. The lattice contraction with no change in the oxidation state of the iron ions suggests the removal of Li and O atoms from the surface of $LiFeO_2$ particles during the first charge process, especially at the plateau region around 4 V. The deficient phase could contribute to the charge and discharge characteristics of the nanoparticles.

To confirm this hypothesis, we directly synthesized the oxygen-vacancy phase $LiFeO_{2-d}$ using *O*3-$LiFeO_2$ nanoparticles and CaH_2 as a reducing agent and compared its structural and electrochemical characteristics with those of $LiFeO_2$ nanoparticles after electrochemical reactions. The reaction is described as follows:

$$LiFeO_2 + xCaH_2 \rightarrow LiFeO_{2-x} + xCaO + xH_2 \quad (1)$$

Fig. 8 shows an XRD pattern and a Mössbauer spectrum of the oxygen-vacancy phase $LiFeO_{2-d}$. Fig. 9 summarizes the lattice parameters and the relative amounts of the $Fe^{3+}(1)$ component in pristine $LiFeO_2$, reduced $LiFeO_{2-d}$, and first charged $LiFeO_2$ nanoparticles. $LiFeO_{2-d}$ had a smaller lattice than pristine $LiFeO_2$. No changes in the oxidation state of Fe^{3+} were observed except for the formation of a slight Fe^{2+} component, whereas the $Fe^{3+}(1)$ ratio was 44:55. These results indicate that the oxygen-deficiency result in cationic rearrangements from the *O*3-$LiFeO_2$ phase to the ordered rocksalt phase. This structural behavior resembles the changes that occur during charging. This supports the results that oxygen ions are released from the *O*3-$LiFeO_2$ phase around the 4.0 V

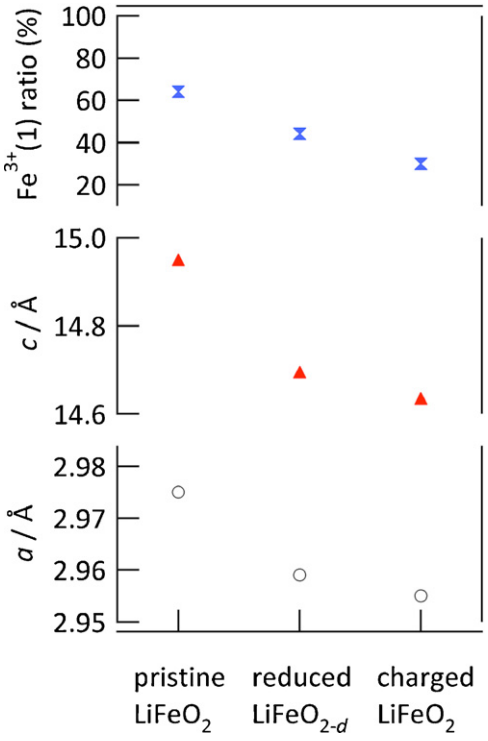

Fig. 9. Lattice parameters and $Fe^{3+}(1)$ ratio of 40-nm $LiFeO_2$: (a) pristine $LiFeO_2$, (b) reduced $LiFeO_{2-d}$, and (c) $LiFeO_2$ charged to 4.5 V.

plateau region during charging. Fig. 10 summarizes the variations of charge/discharge curves for nanosized $LiFeO_2$ and $LiFeO_{2-d}$ during the initial cycles. $LiFeO_{2-d}$ has a shorter plateau region in the first charge curve than $LiFeO_2$. The charge curves of $LiFeO_{2-d}$ after the first cycle do not contain a plateau region. The plateau region around 4 V in the charge curves of $LiFeO_2$ gradually shortened from the first cycle to the 5th cycle. The charge/discharge curves of $LiFeO_2$

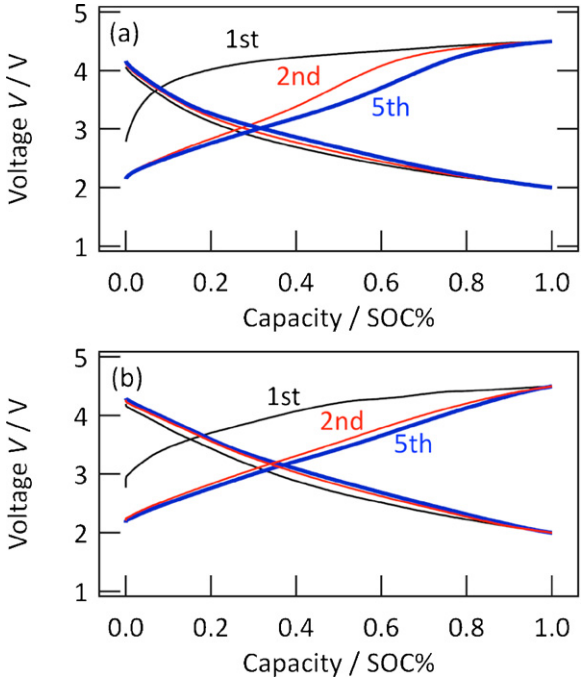

Fig. 10. Charge/discharge curves of $LiFeO_2$ (a) and $LiFeO_{2-d}$ (b) nanoparticles during initial 5 cycles.

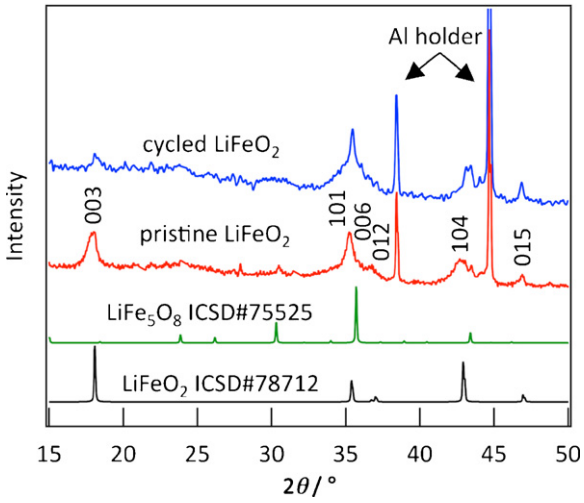

Fig. 11. XRD pattern of 40-nm $LiFeO_2$ after being discharged to 2.0 V at the 23rd cycle. XRD pattern of pristine 40-nm $LiFeO_2$ and simulation XRD patterns of $LiFeO_2$ and $LiFe_5O_8$ based on ICSD data are also shown.

at the 5th cycle are similar to those of $LiFeO_{2-d}$. These experimental results suggest a phase transition from *O*3-$LiFeO_2$ to the oxygen-vacant phase $LiFeO_{2-d}$ during the initial electrochemical cycles. Extraction of oxygen might cause the structure to form a cubic phase that participates in reversible lithium insertion/extraction reactions without altering the valence of Fe^{3+}. This reaction may be reversible for nanoparticles with short diffusion pathways and large surface areas.

The charge/discharge and d*Q*/d*V* curves of $LiFeO_2$ nanoparticles also suggest the phase change in the $LiFeO_2$ nanoparticles after the initial cycles. Fig. 11 shows XRD pattern of 40-nm $LiFeO_2$ after being discharged to 2.0 V at the 23rd cycle. A certain relative intensity changes among the diffraction peaks were observed. The 1 0 1 diffraction peak exhibited the highest intensity for $LiFeO_2$ after 23 cycles, whereas the 0 0 3 diffraction peak exhibited the highest intensity for pristine and first charged $LiFeO_2$. This result indicates a phase transition of the oxygen-vacant $LiFeO_{2-d}$ formed at the initial process. Comparison of the XRD pattern with the ICSD database implies a partial phase transition to $LiFe_5O_8$ ($Li_{0.2}FeO_{1.6}$) with the inverse spinel structure. Considering the formation of oxygen-deficient phase *O*3-$LiFeO_{2-d}$ at the first charge process, the phase transition to the cubic spinel seems to be reasonable. It has been reported by Armstrong et al. that tetragonal $LiFeO_2$ converted to $LiFe_5O_8$ on electrochemical cycling [15]. They also propose that an oxygen loss from tetragonal $LiFeO_2$ occurs due to electrolyte oxidation accompanying charging. However, the charge/discharge behaviors of the *O*3-$LiFeO_2$ nanoparticles differ from those of $LiFe_5O_8$ reported in previous reports [15,16]. $LiFe_5O_8$ electrodes exhibit a slight capacity between 4.5 V and 3.0 V in the discharge curve. In contrast, the *O*3-$LiFeO_2$ nanoparticles after 23 cycles had a plateau region above 3 V. The difference in the voltage of the intercalation reaction indicates that *O*3-$LiFeO_{2-d}$ converts to other phases during the electrochemical cycling. Further structural studies are needed to clarify the crystal structure of the cycled phase.

4. Conclusion

$LiFeO_2$ nanoparticles have been synthesized by the ion-exchange reaction of α-$NaFeO_2$ nanoparticles. The $LiFeO_2$ nanoparticles consist of layered rocksalt *O*3-$LiFeO_2$ and a small amount of the ordered rocksalt phase. An irreversible phase transition to a cubic phase occurs during the first charge process without altering the valence of Fe^{3+}, which indicates that oxygen release contributes to the electrochemical reaction. Oxygen-deficient $LiFeO_2$-d nanoparticles synthesized by reaction with CaH_2 have similar structural and electrochemical properties as the $LiFeO_2$ nanoparticles at the initial process. This demonstrates that oxygen removal causes the structural rearrangements to the cubic phase, which participates in reversible lithium insertion/extraction reactions. The cubic phase exhibit increasing the discharge capacity of over 120 mAh g^{-1} during electrochemical cycling.

Acknowledgments

The authors are grateful to Dr. A. Yamada and Dr. S. Nishimura (University of Tokyo) for their assistance with the Mossbauer measurements. This study was partly supported by a Grant-in-Aid for Scientific Research (A) and a Global COE Program for Energy Sciences, Japan Society for the Promotion of Science.

References

[1] T.A. Hewston, B.L. Chamberland, J. Phys. Chem. Solid 48 (1987) 97–108.
[2] T. Shirane, R. Kanno, Y. Kawamoto, Y. Takeda, M. Takano, T. Kamiyama, F. Izumi, Solid State Ionics 79 (1995) 227–233.
[3] B. Fuchs, S. Kemmlersack, Solid State Ionics 68 (1994) 279–285.
[4] K. Ado, M. Tabuchi, H. Kobayashi, H. Kageyama, O. Nakamura, Y. Inaba, R. Kanno, M. Takagi, Y. Takeda, J. Electrochem. Soc. 144 (1997) L177–L180.
[5] S. Kanzaki, T. Inada, T. Matsumura, N. Sonoyama, A. Yamada, M. Takano, R. Kanno, J. Power Sources 146 (2005) 323–326.
[6] S. Kanzaki, A. Yamada, R. Kanno, J. Power Sources 165 (2007) 403–407.
[7] M. Hirayama, H. Tomita, H. Ido, R. Kanno, The 15th International Meeting on Lithium Batteries Abstracts, 2010, p. 501.
[8] M. Hirayama, H. Tomita, K. Kubota, R. Kanno, submitted.
[9] Y. Tsujimoto, C. Tassel, N. Hayashi, T. Watanabe, H. Kageyama, K. Yoshimura, M. Takano, M. Ceretti, C. Ritter, W. Paulus, Nature 450 (2007) U1062–U1068.
[10] C. Tassel, J.M. Pruneda, N. Hayashi, T. Watanabe, A. Kitada, Y. Tsujimoto, H. Kageyama, K. Yoshimura, M. Takano, M. Nishi, K. Ohoyama, M. Mizumaki, N. Kawamura, J. Iniguez, E. Canadell, J. Am. Chem. Soc. 131 (2009) 221–229.
[11] F. Izumi, T. Ikeda, Mater. Sci. Forum 321 (2000) 198.
[12] F. Izumi, K. Momma, Solid State Phenom. 130 (2007) 15–20.
[13] M. Tabuchi, A. Nakashima, H. Shigemura, K. Ado, H. Kobayashi, H. Sakaebe, H. Kageyama, T. Nakamura, M. Kohzaki, A. Hirano, R. Kanno, J. Electrochem. Soc. 149 (2002) A509–A524.
[14] C.S. Johnson, J.S. Kim, C. Lefief, N. Li, J.T. Vaughey, M.M. Thackeray, Electrochem. Commun. 6 (2004) 1085–1091.
[15] A.R. Armstrong, D.W. Tee, F. La Mantia, P. Novák, P.G. Bruce, J. Am. Chem. Soc. 130 (2008) 3554–3559.
[16] F.O. Ernst, H.K. Kammler, A. Roessler, S.E. Pratsinis, W.J. Stark, J. Ufheil, P. Nov·k, Mater. Chem. Phys. 101 (2007) 372–378.